2D AND 3D-MODELLING OF CONCRETE AS AN ASSEMBLAGE OF SPHERES REVALUATION OF THE FAILURE CRITERION

W.J. Beranek and G.J. Hobbelman
Faculty of Architecture, Delft University of Technology,
The Netherlands

Abstract

For the constitutive modelling of concrete, a physical approach has been chosen. The structure of the material is reduced to its bare essence: an assemblage of equal spheres in their most dense configuration. The spheres are assumed to be rigid, whereas stiffness and strength are concentrated in contact layers of equal thickness between the spheres. A physical failure criterion is introduced; cracks wil develop as soon as the tensile strength in the contact layer is exceeded in whatever direction. For calculation purposes the assemblage of spheres is replaced by an equivalent regular 2D- or 3D-lattice. The mechanical behaviour is basically linear elastic. The model is providing its own failure surface. Non linear effects are introduced by subsequently changing the properties of the members of the lattice in which the failure criterion has been violated.

In the paper a few simple models are reinvestigated, to show the limitations of 2D-models in respect to the location of a regular grid towards the direction of uniaxial tensile and compressive loading. The objective is to obtain a better understanding of the stress transfer in the post peak regime. Results wil be used for a revaluation of the failure criterion for the macro model. Furthermore some failure criteria of other workers with physical models are discussed.

1 Introduction

There are two trends in the constitutive modelling of concrete and other brittle disordered materials :
1   A phenomenological approach; widely used in applied mechanics.
2   A physical approach; more common in the science of materials.
In both methods the mechanical behaviour of a material is determined by a few basic tests. In the first approach, the attention is focussed on the mathematical description of the observed phenomena. But in the second one, the physical explanation of the mechanical behaviour is of primary interest. This second approach seems more promising as one should not only know how things happen but also why they happen.

The finite element method – based on continuum mechanics – is a typical example of a highly mathematical phenomenological approach. It is an excellent tool as long as non linear effects can be neglected. Difficulties are arising however as soon as crack formation has to be simulated. Cracks are smeared out or have to follow a predefined path. Remeshing has also been introduced. In the description of the non linear behaviour in the pre and post peak regime, generally the original finite element configuration is maintained and only the stress-strain relationship is adjusted.

In a physical approach however, the structure of the material has to be introduced. Concrete is then regarded as a two phase material with coarse aggregate particles embedded in a matrix of much softer material. The particles are mostly assumed to have a spherical shape in 3D-problems and are regarded as circular discs in 2D-problems. In a calculation such assemblages are often replaced bij regular or random lattices. They are either treated as trusses in which the members are only transmitting normal forces or as frameworks in which shear forces can be transmitted as well.

The introduction of non linear effects in constitutive models follows the previously described main trends. The phenomenological approach is giving quite convincing load displacement diagrams, but an unsatisfactory crack development as long as no remeshing is introduced. A recently presented physical approach however, is capable of describing a slowly degrading structure of the material. The stress-strain relationship of the material itself remains basically linear elastic but members of the lattice are subsequently removed or provided with new properties after their failure criterion has been violated (Herrmann 1988). Several investigators have applied the latter lattice approach on a micro-scale (Schlangen, van Mier 1992). The crack formation agrees very well with test results in tension and shear, but the load-displacement diagrams are mostly showing a too brittle behaviour. As a consequence both sides claim that something must be essentially wrong with the method they don't use themselves and clarification of this problem is needed. Very promising results however have been obtained by the distinct element method (Vonk 1992).

966

2 Spherical model

Concrete consists of aggregate particles in various shapes and sizes, embedded in a much softer mortar matrix. If a concrete specimen is sawn into two pieces it mostly gives the impression as if the aggregate particles were in suspension in the matrix during the hardening process. More than once such patterns – with the particles on rather large distances – are taken as the starting point for the schematization of concrete. Some researchers try to model the original shape of the larger and medium sized particles, others replace them by spheres having comparable sizes.

In our opinion this is a misleading approach. We strongly feel that concrete should be regarded as a three-dimensional skeleton of larger and smaller aggregate particles, almost in direct contact with each other. The matrix then acts as a filler, capable of transmitting tensile stresses. Furthermore we intend to model concrete on a macro scale. So quite some refinement has to be abandoned and only the essence of the structure of the material should be taken into account. Our starting point is a regular assemblage of equal spheres in their most dense configuration, see fig. 1a (Beranek, Hobbelman, 1991, 1994). The dimensions of these spheres are not supposed to represent the actual sizes of the larger particles.

In this way the continuum is replaced by a semi-continuum. The usual space filling elements of the finite element method are substituted for spherical elements each making contact in twelve points with the other elements, whereas adjoining elements have only one point in common. As a result 74 % of the continuum is replaced by the agregate and the rest by the filler. Due to the much lower modulus of elasticity of the filler, all stresses between the spheres wil mainly be transmitted in the direct vicinity of the contact points between the spheres.

The system lines of such assemblages are the same as those of commonly used space grids. The essence of the configuration is shown in the octahedron of fig. 1b. Triangular grids exist in four sets of planes, parallel to the sides of the octahedron, whereas at the same time square grids exist in three sets of orthogonal planes.
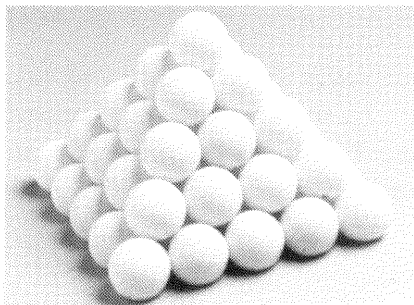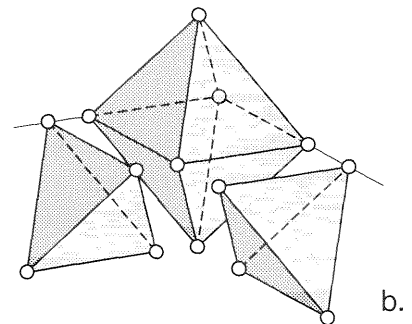
a.   b.

Fig. 1 Similarity between the spherical model and a lattice model
a. Spherical model   b. Octahedron with adjacent tetrahedra

3   Mechanical behaviour of the model

For a description of the mechanical behaviour of concrete, the spheres could have been regarded as elastic bodies, connected by interface elements. But we have preferred a more drastic schematization. The spheres themselves are regarded as rigid. Stiffness and strength are concentrated in elastic contact layers around the contact points of the spheres, with a circular cross section A^* and a thickness t^*, see fig. 2a. Their mechanical behaviour is determined by the elasticity modulus E^* and the shear modulus G^*, with $\psi = G^* / E^*$. The quantities marked with an * have only a meaning for the contact layers themselves.

In a homogeneous state of external stress the normal stresses σ and the shear stresses τ then have to be uniformly distributed over the cross sectional area of each contact layer. They wil cause a normal force N and a shear force Q, both going through the center of the cross section; fig. 2b. The resultant force F will have a line of action, making an angle φ with the system line between the centres of the spheres, see fig. 2a.

The properties of the model are determined in axial tension and compression, just as in continuum mechanics. The behaviour of the material in a 2D-model is characterized by three spheres, in the shape of a triangle, see fig. 2a,b. These spheres will only translate towards each other, but not rotate. The displacement of two spheres towards each other is given by the numerical values of Δn and Δt, with:

$$\Delta t / \Delta n = Q / N \, \psi \tag{1}$$

From the equations of equilibrium and compatability one finds in uniaxial compression the following ratio:

$$\mathrm{tg}\, \varphi = \frac{Q}{N} = \sqrt{3}\, \frac{\psi}{2 + \psi} \tag{2}$$

Poisson's ratio of the configuration proves to be equal to:

$$\nu = \frac{1 - \psi}{3 + \psi} \tag{3}$$

For the time being, the material of the contact layer is assumed to be homogeneous and isotropic in the classical way. As the spheres are assumed to be rigid, no transverse strains can develop. From this condition ψ can be expressed in Poisson's ratio ν^* of the contact layer as follows:

$$\psi = \frac{1 - 2\nu^*}{2\,(1 - \nu^*)} \tag{4}$$

The numerical value of ν^* is treated as one of the basic parameters of the model, which should only be used for $0 \leq \nu^* \leq 0.2$.

968

4 Equivalent lattice model

Any spherical model can be replaced by an equivalent space grid (lattice model) along the system lines of the spherical model, see fig. 2c. The members have to be rigidly connected to each other in the nodes, which are not allowed to rotate towards each other, so $Q\,a\ =\ 2\,M$, see fig. 2c. The normal stiffness EA and the bending stiffness EI of the members have to be chosen in such way, that under the same external load the same displacements will occur as in the spherical model, which in their turn should represent reality. The displacement of two spheres towards each other is given by the numerical values of Δn and Δt, with:

$$\frac{\Delta t}{\Delta n} \ = \ \frac{A\,a^2}{12\,I}\,\frac{Q}{N} \tag{5}$$

Substitution of (5) in (1) gives the following relationship between A and I of the member:

$$I \ = \ \frac{\psi}{12}\,A\,a^2 \tag{6}$$

From equation (6) it follows that the radius r of a circular cross section or the height h of a rectangular one, are respectively equal to:

$$r \ = \ \frac{\sqrt{3}}{3}\,a\,\sqrt{\psi} \quad \text{and} \quad h = a\,\sqrt{\psi} \tag{7a, b}$$

In equation (7b) the width b of the member is chosen equal to the width of the model. Furthermore one can assume that $E_{\,member} = E_{\,concrete}$, as differences are negligible.
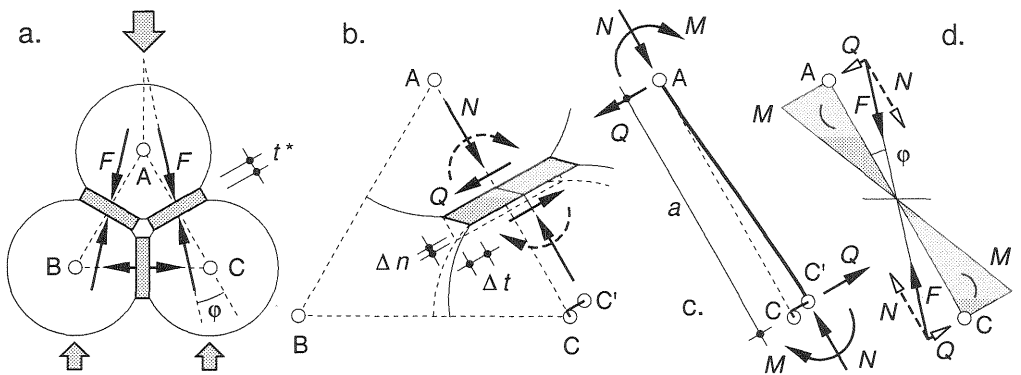

Fig. 2 Replacement of the spherical model by an equivalent lattice model
a. Basic unit of three spheres in uniaxial compression
b. Displacements of the contact layer subjected to forces from the spheres
c. Displacements of the member of the lattice due to forces in the nodes
d. Bending moment in the member and thrustline of the member

5   Failure criterion

Failure of concrete is always caused by cracking. So a linear stress-strain relationship is assumed in which only the uniaxial tensile strength f_t is defined, see fig. 3a. Cracks are supposed to occur as soon as the tensile strength in the contact layer is reached in one or another direction. In the contact layer no transverse strains are possible as the spheres are assumed to be rigid. This leads to the following ratio η between the transverse stresses and the normal stress, see fig. 3b:

$$\eta = \frac{\sigma_{ss}}{\sigma_{nn}} = \frac{\sigma_{tt}}{\sigma_{nn}} = \frac{v^*}{1 - v^*} \tag{8}$$

In fig. 3c some Mohr's circles are shown all having the same principal tensile stress, which is taken equal to the tensile strength f_t. The matching normal and transverse stresses are obeying equation (8). So each circle represents a combination of normal stress σ_{nn} and shear stress σ_{nt} which will cause failure, see fig. 3b. The critical shear stress can be expressed as:

$$\sigma_{nt} = \pm \sqrt{f_t^2 - f_t(\eta + 1)\sigma_{nn} + \eta\, \sigma_{nn}^2} \tag{9}$$

Equation (9) represents a hyperbola with the origin of the coordinate system in a focus, with the asymptotes under an angle ϕ with $\mathrm{tg}\,\phi = \pm \sqrt{\eta}$., see fig. 3d. In fig. 3c also the crack direction in the contact layer is shown, which is hardly changing in mode II: compression + shear.
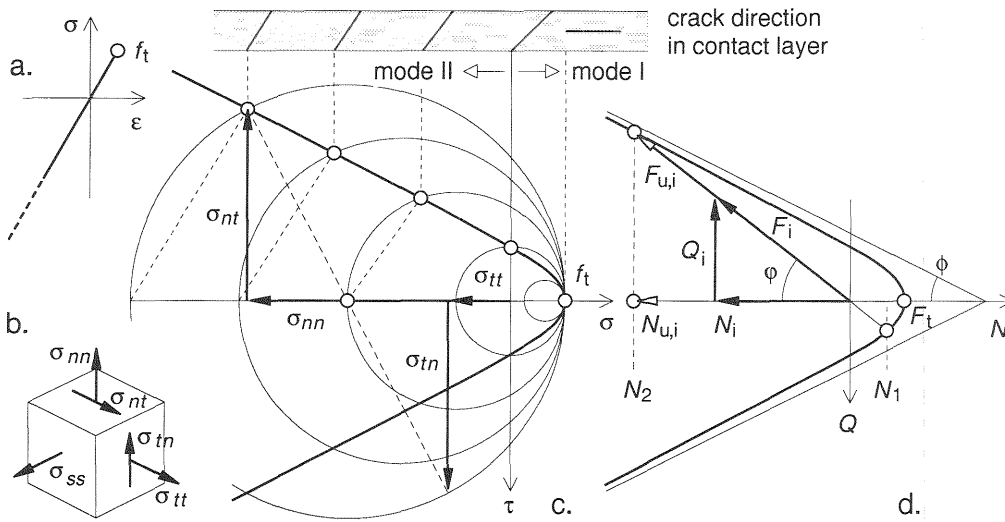

Fig. 3   Failure criterion for the contact layer $(v^* = 0.2)$
a.   Stress-strain relationship
b.   Normal and transverse stresses
c.   Failure contour for $\eta = 0.25$
d.   Determination of the factor ϑ

So a strict application of Mohr's circles leads to a criterion which is very alike the linear relationship between compression and shear which follows from the assumptions of Coulomb, whereas the strength in tension is the same as in shear, just as Coulomb also suggested (Timoshenko 1953). The usual interpretation however – designated as 'Mohr-Coulomb' with the traditional tension cut-off – has become meaningless in this approach.

In the lattice model the same formula can be used when the stresses and strength are replaced by the forces N, Q and F_t, see fig. 3d. In the calculation of a model the resulting force F_i in each member is compared with its value at failure $F_{u,i}$. The ratio between the two is designated as:

$$\vartheta_i = \frac{F_i}{F_{u,i}} \ 100\% = \frac{N_i}{N_{u,i}} \ 100\% \tag{10}$$

So it is sufficient to determine the extreme values of N for each member:

$$N_{1,2} = \frac{1}{2} F_t \ \frac{-(\eta + 1) \pm \sqrt{(\eta + 1)^2 + 4\,(\mathrm{tg}^2\varphi - \eta)}}{\mathrm{tg}^2\varphi - \eta} \tag{11}$$

6   Comparison with results from literature

In a 2D-model the behaviour is characterized by a basic configuration in the shape of a triangle and in a 3D-model in the shape of a tetrahedron, see fig 1b. Subjecting these configurations to external biaxial principal states of stress gives failure contours which show all the essential features of the failure contour according to Griffith for the 2D-model and of the failure contour according to Kupfer for the 3D-model. In the last case external triaxial states of principal stress can be applied just as easily to obtain a complete failure surface (Beranek, Hobbelman 1993).

The essential step forward in describing failure is credited to the fact that each biaxial state of stress is now resolved into three uniaxial stresses and each triaxial state of stress into six uniaxial stresses. In the lattice model these uniaxial stresses are represented by the resulting forces F, acting along their thrustlines. These stresses – and their resulting forces – have to be held responsible for failure as the bond between agregate and matrix is the weakest point in concrete. So halfway each member the criteria according to the formulas (9) and (11) are valid and only at these cross sections the bond can be broken. The bending moment in the member is only required to guarantee the correct boundary conditions halfway the member. It has no meaning at the nodal points themselves. In a non homogeneous state of external stress however, the value of the bending moment will generally be unequal to zero at the governing cross section and still has to be taken into account somehow.

Lattices which are treated as trusses are hardly suitable to describe the behaviour of concrete. Not only is Poisson ratio equal to 1/3, but in a regular lattice is the tensile strength just 1/3 of the compressive strength. Lattices as proposed by Herrmann (1988) however, are an ideal starting point to model concrete. Especially van Mier and co-workers have extensively used such lattices, comparing the numerical results with their own test results. They claim an excellent agreement in crack development, but have to admit a too brittle behaviour. They obtained the dimensions of their members by curve fitting. In their approach the failure criterion is based on elementary beam theory where cracks are supposed to occur as soon as the extreme tensile stress, determined from $\sigma = N/A \pm M/W$, has reached the tensile strength. It will be obvious that this formula may be perfectly suited for steel or concrete frames, but not for the simulation of a semi-continuum like concrete. So they introduced correction factors α and β in their stress criterion and determined the numerical values by tuning with test results. Their formula reads (Schlangen, van Mier 1992) :

$$\sigma_{i,j} = \beta \left[\frac{N}{A} \pm \alpha \frac{M_{i,j}}{W} \right] \tag{12}$$

In tension plus shear they adopted the values $\alpha = 1/3$ and $\beta = 2$. The question arises which link can be laid between their criterion given in (12) and ours in (9). First of all, in a 2D-model with rectangular beams having a cross section $A = b \times h$ (b = width of the model), they have introduced for the height of the beam element: $h = 0,68\ a$ (a = beam length).

Substitution of $v^* = 0.1$ in (4) results in $\psi = 4/9$, which in its turn leads to $h = 2/3*a$ according to (7b). As the geometry of the two grids is practically the same, the mechanical behaviour should also be the same. For a fair comparison the tensile strength in both models should be equal, which leads to $\beta = 1$ in (12). In each homogeneous state of external stress one finds $M = Q*a/2$. Equation (12) can further be rewritten by the following substitutions: $A\sigma = Af_t = F_t$; $W = 1/6*bh^2$; $a = 3/2*h$. This leads to a failure criterion which is expressed in N, Q and F_t:

$$F_t = N \pm 3\alpha \frac{3}{2} Q \tag{12a}$$

In fig. 4 the criterion according to (12a) is shown for $\alpha = 1/3$, which can be interpreted as critical cross sections on distances of $1/3a$ from the nodes. The failure criterion according to (9) is also expressed in N and Q:

$$Q = \pm \sqrt{F_t^2 - (\eta + 1) F_t N + \eta N^2} \tag{9a}$$

This failure contour is shown in fig. 4 for two values: $\eta = 1/9$ ($v^* = 0.1$) and $\eta = 1/4$ ($v^* = 0.2$). The straight lines according to van Mier give the impression of a linear best fit curve for both hyperbolas.
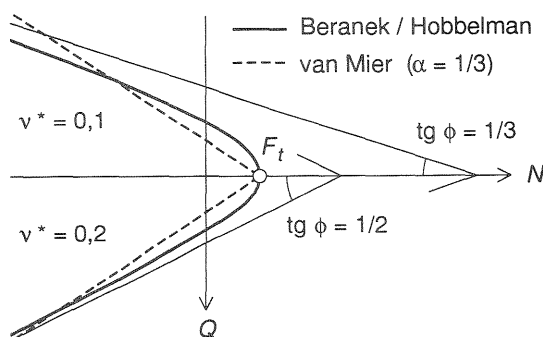
972

Fig. 4 Comparison of the failure criteria according to equation (9a) and (12a)
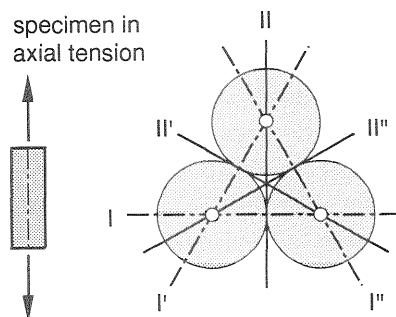
Fig. 5 Triangular grid with orthogonal directions I and II

7 Calculation technique

Calculations have been carried out with a standard framework program without applying any alterations. All the work has been concentrated on pre-, inter- and post-processing. For 2D-models only regular triangular lattices have been applied, whith one of the two orthogonal main directions parallel to the axis of the model, see fig. 5. All calculations are carried out for a prescribed external load or a prescribed displacement and calculations are basically linear elastic. After the first calculation the ratio $\vartheta = F_i / F_{u,i} * 100 \%$ is determined for all members of the grid. The highest value ϑ_{max} is selected and the external load or prescribed displacement is multiplied with a factor $100 / \vartheta_{max}$, which will just produce failure in the most affected member of the lattice, whereas all other members still are obeying the failure criterion. We find it most convenient to reproduce all resulting forces F for each loading case into the failure criterion, as it gives an exellent overview of the state of internal stress the model is submitted to, see fig. 6c. In the case of tension – with or without shear – in the most affected member, brittle failure is assumed to occur and the member should be removed from the grid. For practical reasons the values of the cross sectional area A and the second moment of area I are reduced to 0.001 % of their original value. Now the calculation is started again with the slightly altered configuration of the grid and the next member is determined in which the failure criterion is violated. The whole procedure is repeated untill the load bearing capacity of the model is exhausted. From the calculation a displacement is selected which is governing the problem and plotted against the matching external load or prescribed displacement. This leads to quite unusual load-displacement diagrams, see fig. 7. Contours can be drawn for increasing load or displacement – hiding all the snap-backs – but the original plot of data gives considerably more information about the degrading model.

973

Most investigators apply lattice models on a meso scale ($a = 1$-10 mm) and often random values are introduced for length, strength and stiffness of the members of the grid. Attention is focussed on crack development and load-displacement diagrams. The stress distribution is seldom shown.

We want to apply the model basically on a macro scale. The maximum member length is then governed by the minimum crack distance in tension which one still wants to record, so member lengths of 50 mm and more are quite common. This results in stylized crack patterns in which nevertheless such phenomena as micro cracking, strain softening and aggregate interlock are shown in a condensed way. A thorough analysis of the mechanical behaviour however, requires a recording of the flow of forces during the complete loading history of a model. This has been the main reason to stick to complete regularity in the model. Only then a logical explanation of the phenomena wil be traceble, which otherwise might remain hidden in the scatter of results. This is especially the case as long as the failure criteria are still under investigation and numerical results have to be compared with test results. In each loading step a visualization of the forces between the spheres can be produced at wil, together with the crack development, see fig. 6. Due to the regularity of the lattice, these forces can be interpreted as uniaxial stresses in magnitude and direction.

To demonstrate the potential of the method, as wel as the limitations, the results are shown of three uniaxial tensile tests on prismatic specimen. In fig. 6a, b the axis of the specimen is parallel to a main direction I and in fig. 6c parallel to a main direction II, see fig. 5. In fig. 6a the load is introduced by rigid non rotatable loading platens, and in fig. 6b,c by rigid loading platens which may rotate freely. Transverse displacements at the loading platens, due to Poisson's ratio, are not prevented however.

For each specimen the following data are shown (for tg $\phi = 1/2$):

1. 2. The forces F between the spheres in magnitude and direction (shown as direction and width of rectangular blocks) together with the location of the cracks, shortly after the beginning of cracking and later.

3. The failure criterion with magnitude and direction of all forces F_i between the spheres for the cases 1. and 2. Furthermore the crack width for case 2. and the load displacement diagram with the location of the loading cases 1. and 2.

Only a small part in the middle of the specimen is shown where the cracks are developing. As the figures are rather small, the shape of the spheres is not shown and only the gridlines are reproduced. Tensile forces are shown in black, compressive forces in grey and cracks by smal longer rectangles perpendicular to the grid. Due to the pronounced directions of the grid and the external load, some phenomena are dominant present in one figure but completely absent in another one. A carefull study of the subsequent loading cases is most enlightening. It explains the mechanical behaviour of the specimen and confirms observations from tests (Hordijk 1991).
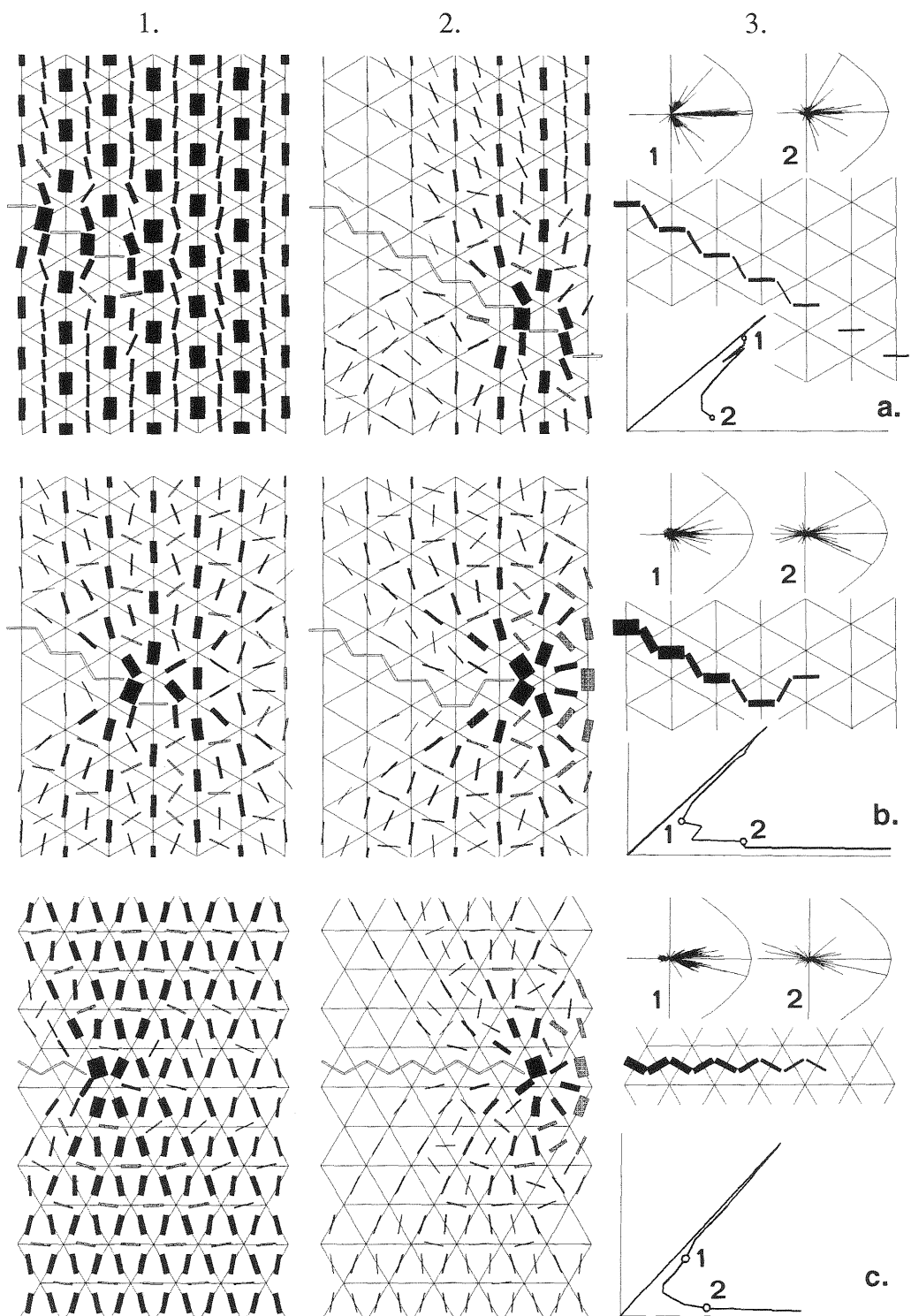
Fig. 6   Axial tension of a prismatic specimen (description previous page)
a.   Non rotatable loading platens;   b. c.   Rotatable loading platens

To enforce crack formation in the middel part of the specimen and not at the loading platens, one member along the edge has been given a reduced tensile strength of 90 %. In fig. 6a all forces in the undisturbed region are almost parallel to the axis of the specimen. Plane sections remain plane but forces in pure tension are much larger than forces in tension + shear, causing alternating bands of high and low forces, see fig. 6a1. Crack formation starts with micro cracking, i.e. non through going cracks, as the slightly loaded members are capable of taking over the load from the cracked members in pure tension. The position of the grid is stimulating a diagonal band of micro cracks over the whole width of the specimen before a through going crack is starting from left to right, subsequently connecting the individual micro cracks. The statically indeterminate boundary conditions are causing a transverse shift of the original axial load.

In fig. 6b the specimen remains axially loaded at the boundaries, but this implies that a cracked cross section has to transmit a resultant tensile force as well as a bending moment. In the undisturbed region the phenomena are similar to those in fig. 6a, but now there is only a slight amount of micro cracking. Already after the second micro crack a macro crack is starting to develop. The crack path is not longer fully determined by the diagonal grid band as in fig. 6a, but it goes on zig-zagging, basically perpendicular to the free uncracked edge. Note also the forces at the crack tip, one of them reaching the tensile strength, the almost stress free edges in fig. 6b1 and the considerable compressive forces in fig. 6b2.

In fig. 6c the boundary conditions are the same as in fig. 6b, but as the direction of the grid has changed, all members in tension must also transmit shear forces, which causes small compressive forces in tranverse direction. The possibility of micro cracking with a gradual redistribution of forces now has completely vanished. The first tensile crack is appearing at a much higher external load than in the previous cases, just as an elementary calculation predicts. But the drop in loading capacity after the appearance of the first crack is also much greater than in the previous cases. The crack can now easily follow a horizontal band, but the stress distribution around the crack tip and at the free edge is quite similar to that of the previous case, compare fig. 6c2 with fig. 6b2.

8   Crack development in compression plus shear

In compression plus shear the idea of brittle breaking beams must be abandoned and a more ductile behaviour is required, as a slowly degrading structure still can support increasing loads. A completely cracked and disrupted specimen wil even be capable to support large loads if it is under triaxial compression. So it seems reasonable to maintain the normal stiffness EA and adapt only the bending stiffness EI of the members.

The degrading qualities of the concrete can be taken into account fourfold, (Beranek, Hobbelman 1994 b). As the chosen structure of the model is too coarse to describe complete disrupture, a non linear stress-strain relationship could be introduced . Furthermore every time the failure criterion is violated in a member, the value of EI is stepwise reduced whereas at the same time the tensile strength F_t in the failure contour for that member is also stepwise reduced. This means that at last the cohesion in the failure contour will become zero and a condition of pure friction remains. Finally a compression cut-off (crushing cut-off) can be implemented.

The behaviour of the concrete is varying from very brittle to ductile, depending of the way these reduction factors are chosen. At the moment the best way seems to compare the numerical results of various combinations with test results and make a pragmatic choise. In fig. 7 some first results are shown of a square specimen under axial compression in direction I of the grid. First of all the bond is broken in all horizontal members which are under tension. After that the load will increase and failure in mode II is starting. At first sight the stress distribution has hardly changed, but the two outer parts of the specicmen are shearing off as can easily be deducted from the crack pattern (mode I in black and mode II in grey).
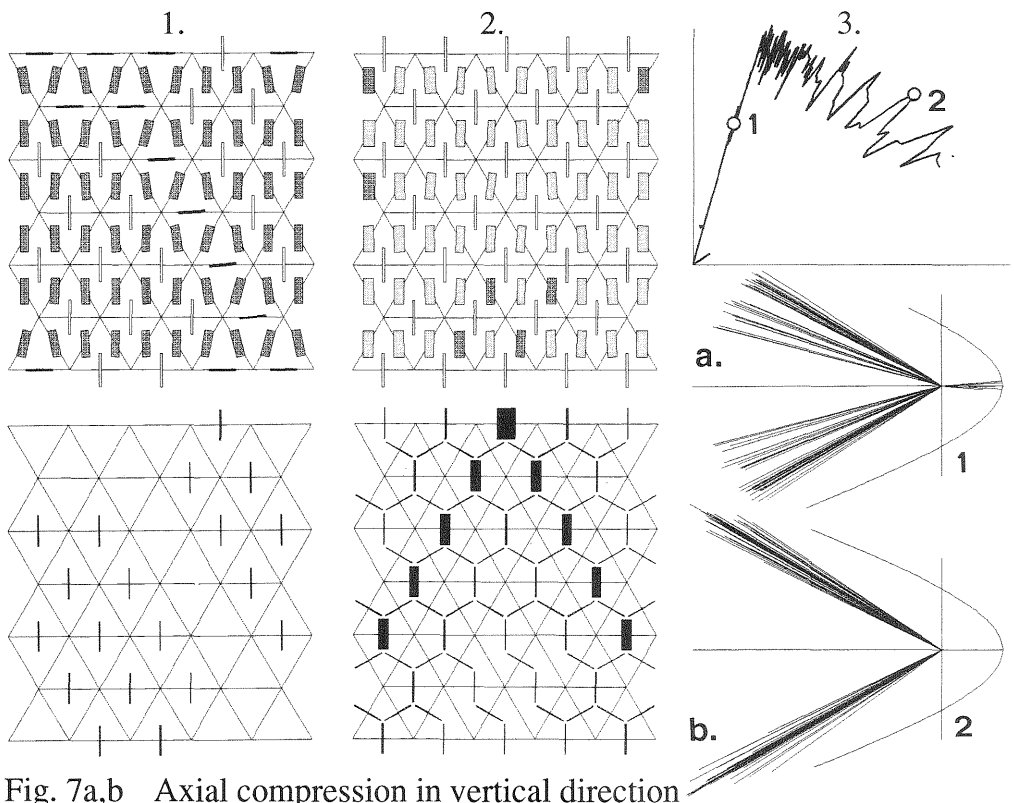

Fig. 7a,b   Axial compression in vertical direction
a.   Force distribution (1.; 2.) and load-displacement diagram (3.)
b.   Crack width (1.; 2.) and failure contour with all forces F_i (3.)

9   Conclusions

The structure of concrete has been introduced as a regular assemblage of equal spheres. Calculations are carried out on an equivalent two or three-dimensional grid (lattice). With a failure contour for one bond between two spheres as a basis, the model is capable of automatically producing a three dimensional failure surface for bi- and triaxial stress conditions.

The mechanical behaviour is shown in a condensed and stylized way, but phenomena as micro-cracking with its subsequent tension softening; discrete macro cracking in whatever direction and aggregate interlock are easily recognised. Due to the introduced visualization techniques the flow of forces is easily understandable.

Discrete crack formation in mode I and II can be realized in a realistic physical way and load displacement diagrams can be brought into agreement with test results. Further research is required however, especially in uniaxial compression when gridlines are parallel to the axis of a specimen.

References

Beranek, W.J., Hobbelman, G.J. (1991) A mechanical model for brittle materials, Proc. of the 9th Int. Brick/Block Masonry Conf., Berlin, Deutsche Gesellschaft für Mauerwerksbau, Bonn, 694 - 702.

Beranek, W.J., Hobbelman, G.J. (1993) A new constitutive model for brick, mortar and masonry, Computer Methods in Structural Masonry II, Books & Journals Int. Ltd Swansea, 38 - 49.

Beranek, W.J., Hobbelman, G.J. (1994 a) Constitutive modelling of structural concrete as an assemblage of spheres, in Computational Modelling of Concrete Structures, Pineridge Press Ltd, 37 - 51.

Beranek, W.J., Hobbelman, G.J. (1994 b) Modelling of masonry as an assemblage of spheres on various scales, Proc. of the 10th International. Brick /Block Masonry Conf., Calgary, Vol . 1, 1 - 10.

Herrmann, H.J. (1988) Introduction to modern ideas on fracture patterns, in: Random fluctuations and pattern growth, Kluver Dordrecht.

Hordijk, D.A., (1991), Local approach to fatigue of concrete, Ph. D thesis, Delft University of Technology, Meinema b.v. Delft

Schlangen E., van Mier, J.G.M. (1992), Micromechanical Analysis of Fracture of Concrete, Int. Journal of damage mechanics, Vol 1- october 1992, 435-454.

Timoshenko, S.P. , History of Strength of Materials, McGraw-Hill, New York, 1953, pp. 47-51.

Vonk, R. (1992) Softening of concrete loaded in compression, Ph. D Thesis, Eindhoven University for Technology